RESEARCH ARTICLE

VOLCANICA

Spatial analysis of globally detected volcanic lightning from the June 2019 eruption of Raikoke volcano, Kuril Islands

Cassandra M. Smith*[α], Alexa R. Van Eaton[β], David J. Schneider[α], Larry Mastin[β], Robin S. Matoza[γ], Kathleen McKee[δ,ε], and Sean Maher[ζ]

[α] U.S. Geological Survey, Alaska Volcano Observatory, Anchorage, Alaska USA.
[β] U.S. Geological Survey, Cascades Volcano Observatory, Vancouver, Washington USA.
[γ] Department of Earth Science and Earth Research Institute, University of California, Santa Barbara, Santa Barbara, California, USA.
[δ] Climate and Radiation Laboratory, Earth Science Division, NASA Goddard Space Flight Center, Greenbelt, Maryland, USA.
[ε] University of Maryland Baltimore County, Baltimore, Maryland, USA.
[ζ] U.S. Geological Survey, California Volcano Observatory, Moffett Field, California USA.

Abstract

The 21–22 June 2019 eruption of Raikoke volcano, Russia, provided an opportunity to explore how spatial trends in volcanic lightning locations provide insights into pulsatory eruption dynamics. Using satellite-derived plume heights, we examine the development of lightning detected by Vaisala's Global Lightning Dataset (GLD360) from eleven, closely spaced eruptive pulses. Results from one-dimensional plume modeling show that the eruptive pulses with maximum heights 9–16.5 km above sea level were capable of producing ice in the upper troposphere, which contributed variably to electrification and volcanic lightning. A key finding is that lightning locations not only followed the main dispersal direction of these ash plumes, but also tracked a lower-level cloud derived from pyroclastic density currents. We show a positive relationship between umbrella cloud expansion and the area over which lightning occurs (the 'lightning footprint'). These observations suggest useful metrics to characterize ongoing eruptive activity in near real-time.

Plain-language summary

Raikoke volcano in Russia's Kuril Islands erupted from 21–22 June 2019. We use observations from satellite, globally detected lightning, volcanic plume modeling, and infrasound to analyze this eruption. We show clear spatial and temporal relationships between the lightning and the development of both (1) the high-altitude volcanic plume that was blown east-southeast and (2) lower altitude ash clouds that traveled northwest. Additionally, we show that as the ash cloud increases in size, the area in which lightning occurs also increases in size. These findings may provide useful ways to use near real-time lightning data for volcano monitoring.

Keywords: Volcanic Lightning; Plume Modeling; GLD360; Plumeria.

1 Introduction

Volcanic lightning has been shown to be a promising tool for monitoring remote volcanoes because it can be detected by existing networks with global coverage and provides evidence of high-intensity or high-altitude volcanic plumes. Previous work has revealed relationships between plume dynamics, microphysical properties, and the generation of volcanic lightning [Mather and Harrison 2006; James et al. 2008; McNutt and Williams 2010; Woodhouse and Behnke 2014; Carey et al. 2019; Nicoll et al. 2019; Méndez Harper et al. 2020; Prata et al. 2020; Van Eaton et al. 2020; 2022]. However, fundamental questions remain about how to best interpret and apply lightning detection to characterize explosive eruptions [Mather and Harrison 2006; Behnke and McNutt 2014]. In particular, relationships between the spatial characteristics of volcanic lightning locations and the plume's travel direction, spatial dimensions, and vertical distribution are not well developed.

Over the past decade, globally detected volcanic lightning has been studied in several large-scale eruptions, forging connections between lightning activity and ice generation at freezing levels of the atmosphere [Behnke et al. 2013; Hargie et al. 2019; Prata et al. 2020; Van Eaton et al. 2020; 2022]. Lightning rates also show a positive correlation with mass eruption rate and plume height [Van Eaton et al. 2016; Prata et al. 2020; Smith et al. 2021; Van Eaton et al. 2022]. These studies parallel existing meteorological models that indicate the importance of ice and strong updrafts for lightning activity in regular thunderstorms [Williams et al. 1989; Saunders et al. 2006; Deierling et al. 2008; Buiat et al. 2017; Schultz et al. 2017]. Several papers, including those examining the eruptions of Kelud, Indonesia [Hargie et al. 2019], Calbuco, Chile [Van Eaton et al. 2016], Redoubt, USA [Behnke et al. 2013], and Bogoslof, USA [Smith et al. 2018; Van Eaton et al. 2020] volcanoes, have also examined general spatial trends of globally detected lightning locations. Overall, these spatial analyses showed that lightning occurring farther away from the volcanic vent was likely related to ice charging and followed the ice particulates' travel direction. Hoblitt [1994] and Van Eaton et al. [2016] also suggested the possibility of lightning being generated by, and spatially aligning with, ash elutriated from ground-hugging pyroclastic density currents (PDCs).

The June 2019 eruption of Raikoke volcano in the Kuril Islands, Russia, provided a superb opportunity to examine these

*smithcm09@gmail.com

Editor: O. Lamb | Typesetter: J. Farquharson

trends. Raikoke is a remote oceanic stratovolcano—its top rises 550 m above sea level as an island that is visibly 2.7 × 2.6 km across [Levin et al. 2010; Smirnov et al. 2021]. Prior to 2019 there had been two major historic eruptions (in 1778 and 1924). During the 2019 eruption there were no monitoring instruments located directly on the island [Girina et al. 2019; Firstov et al. 2020]. Thus, remote observations from satellite, infrasound, and volcanic lightning were particularly valuable for detecting and characterizing this eruption [Horváth et al. 2021; McKee et al. 2021]. The 2019 eruption began on 21 June, producing several short-lived eruptive pulses over a period of 16 hours—each creating a distinct phase of lightning activity [Firstov et al. 2020; McKee et al. 2021]. The resulting ash clouds covered an estimated 227,000 km^2 of airspace and became a significant hazard to aviation [Degterev and Chibisova 2020]. In this paper we examine the spatial distribution of Raikoke's volcanic lightning, how it changed throughout the eruption, and how these features relate to the plume dynamics and microphysics revealed through satellite observations and one-dimensional (1-D) plume modeling.

2 Methods

2.1 Eruption cloud analysis

We used satellite observations from Himawari-8 (operated by the Japan Meteorological Agency) combined with atmospheric weather data and 1-D volcanic plume modeling to analyze eruption clouds from the 2019 eruption of Raikoke volcano. Note that we use the terms eruption cloud, column, and plume interchangeably in this study. Himawari-8 is a geostationary weather satellite that records multispectral images every 10 minutes, which provided good coverage of the eruptive activity from 21–22 June 2019. Using band 13 thermal infrared (10.4 µm) brightness temperatures, we manually picked the coldest pixel (2 km resolution) in each image within a box spanning 20 km W, 20 km S, 40 km N, and 40 km E of the volcano. This rectangular bounding area was used because strong winds advected the plumes east and north. Global atmospheric data from the ERA-Interim reanalysis [Dee et al. 2011], interpolated over the volcano, were used to match the minimum satellite brightness temperatures to a corresponding height from the atmospheric temperature profile (Supplementary Material 1; Figure S1). We recognize that this method represents an oversimplification for clouds that reached the stratosphere (>11 km above sea level); however, in this case our results agree reasonably well with plume heights derived from more sophisticated approaches [Horváth et al. 2021].

ERA-Interim wind profiles were also used to correlate the movement of the eruption clouds with altitude. Eruption clouds seen in the satellite images are generally moving east, away from Raikoke volcano, which is consistent with moderate winds (~20 $m\,s^{-1}$) at altitudes above ~2 km. Below 2 km, the winds blew to the northwest and west at up to 5 $m\,s^{-1}$. Where feasible, we determined the radius of the growing umbrella cloud region for each eruptive pulse. Umbrella cloud areas were determined from the −20 °C isotherm in Himawari-8 band 13 images; areas were then converted to area-equivalent circular radius. Where the cloud was windblown and partly merged into remnants of a previous eruptive pulse, the boundaries were visually estimated.

We used the empirical plume height scaling relationship developed by Sparks et al. [1997] and Mastin et al. [2009] in the form of Equation 2 provided in Mastin [2014] to calculate the mass eruption rate corresponding to each plume height. The 1-D volcanic plume model `Plumeria` [Mastin 2007; 2014] was used to further constrain eruption source parameters for each eruptive pulse. `Plumeria` is an integral plume model that calculates bulk properties of a steady-state plume as a function of height, assuming conservation of mass, momentum, and energy [Mastin 2007]. The model also accounts for effects of a crosswind [Mastin 2014], which was important for Raikoke's wind-swept plumes. We used atmospheric sounding measurements from Severo-Kurilsk, Russia (~340 km NE of volcano) for the atmospheric inputs to `Plumeria`. These sounding data are consistent with the ERA-Interim reanalysis used for plume height determinations, as shown in Supplementary Material 1 (Figure S1). We varied the diameter of the vent throughout the eruption from 50–150 m and the exit velocity between 50–200 $m\,s^{-1}$ to obtain the observed plume heights for each of the eruptive pulses. The source parameters used for modeling are shown in Supplementary Material 1 (Table S1).

2.2 Volcanic lightning analysis

Lightning strokes were obtained from Vaisala's Global Lightning Dataset (GLD360) [Said and Murphy 2016] within a 300 km radius around Raikoke volcano. To locate lightning, the GLD360 system uses very low frequency signals emitted from cloud-to-ground (CG) return strokes and in-cloud (IC) k-strokes, which represent the part of the lightning flash that transfers a large amount of charge from either the cloud to the ground or between clouds [Said and Murphy 2016]. The large 300 km radius around Raikoke volcano was chosen to capture lightning in the eastward drifting eruption clouds. The lightning catalog was compared to the Himawari-8 visible satellite data, and we identified 92 strokes that occurred more than 80 km outside the visible plume boundaries to the north and west—these strokes were discarded from the volcanic lightning dataset as they did not spatially align with the volcano or the eruption clouds. This analysis resulted in a count of 753 total lightning strokes for the eruption. Each stroke has an associated time, two-dimensional location (latitude and longitude but not height) and estimated peak current and polarity (Figures 1 and 2, Supplementary Material 2). Vaisala provided information on location errors, and due to the distribution of sensors in this region of the GLD360 lightning network, strokes had elliptical location errors with minor and major axes of 1.5 × 6.2 km rotated 41 degrees counterclockwise, resulting in error ellipses with a northwest–southeast trend (Figure 1). Individual lightning strokes may be grouped into 'parent' flashes by combining the strokes that occur within a set time and distance. For simplicity in this analysis, we use strokes rather than flashes, but the flash rates are also included in Supplementary Material 3 (using 1 s and 20 km to group individual strokes into parent flashes [Said et al. 2010; Van Eaton et al. 2022]). We classified strokes as CG or IC based on the study

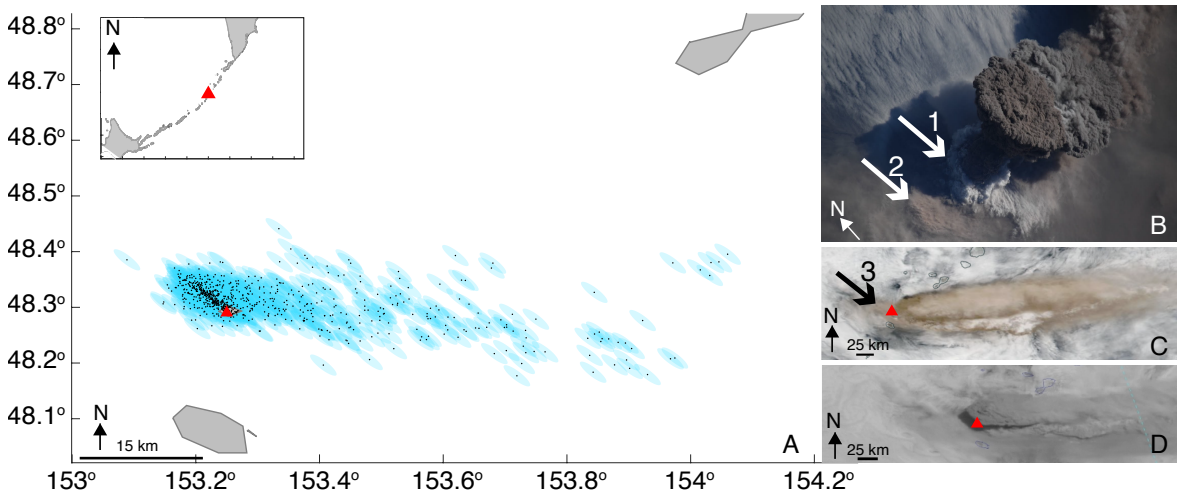

Figure 1: [A] Map of Raikoke volcano (red triangle) and volcanic lightning locations from 21-22 June 2019 (black dots) with associated location uncertainties (blue ellipses). Images show eruptive pulse 7 captured from [B] the International Space Station at 22:46 UTC on 21 June (NASA photo ID ISS059-E-119250 – no scale provided), [C] true color Suomi NPP/VIIRS, and [D] Himawari-8 visible/band 3. Arrow 1 points to clouds associated with ground-hugging pyroclastic density currents that enveloped the island (Smirnov et al., 2021); arrows 2 and 3 point to a low-level ash cloud traveling to the northwest.

of Biagi et al. [2007], who found that peak current magnitudes >15 kA were statistically more likely to represent CG lightning (their study showed that ~95 % of lightning >20 kA was CG). In the absence of more detailed waveform data, we classified strokes with peak currents greater than ±15 kA as CG. This simplifying assumption is consistent with previous work on lightning classification [Cummins and Murphy 2009; Rudlosky and Fuelberg 2010; Schultz et al. 2011]. Lightning stroke rates were calculated in 10-minute bins to match the temporal resolution of the Himawari-8 satellite images. For each 10-minute period with three or more lightning strokes, a concave hull (the smallest polygon enclosing all points) was manually outlined in the program `ImageJ` [Rueden et al. 2017]. The area of this polygon was used to calculate the area-equivalent circular radius of the lightning spatial footprint for each 10-minute period (Supplementary Material 3).

3 Results

Our analysis demonstrates that Raikoke volcano's high-intensity explosive activity took place over ~16 hours as a series of 11 eruptive pulses. Each eruptive pulse formed discrete ash plumes and associated lightning activity, punctuated by short time breaks (Figure 3 and Supplementary Material 1; Table S1). Plume heights ranged from 3.7–16.5 km above sea level, which is similar to the range of heights reported by Horváth et al. [2021] (4.8–16.7 km) and Kloss et al. [2021] (9–16 km). During the largest eruptive pulse (pulse 7) the coldest pixel in satellite imagery was −55.9 °C, which is a few degrees colder than the atmospheric profile, indicating that the plume top was undercooled. For these undercooled values, we simply used the coldest temperature in the atmospheric profile from ERA-Interim reanalysis. Despite this simplification, our resulting stratospheric injection height is consistent with independent estimates by Horváth et al. [2021] and Kloss et al. [2021].

The seventh, and largest, eruptive pulse was captured in several images shown in Figure 1. An astronaut photograph taken from the International Space Station (Figure 1B) reveals low altitude, white clouds rising from pyroclastic density currents that flowed in all directions down the slopes of the volcano (documented by Smirnov et al. [2021]) as well as low-level brownish clouds to the west-northwest. A VIIRS image also shows a brownish cloud to the west-northwest (arrow in Figure 1C), which we interpret as ash lofted from the ground-hugging pyroclastic density currents and blown by low altitude winds. In Figure 1B there is no evidence of the column being advected at low levels; the edges of the column look sharply defined, supporting our interpretation of this cloud originating from the PDCs. During eruptive pulse 7, lightning was detected both to the northwest and to the east of Raikoke volcano (Figures 1 and 4). The location of all lightning strokes and corresponding error ellipses are shown in Figure 1A. However, even taking the location uncertainties into consideration, the strokes appear to follow two main dispersal axes—one northwest of the volcano and another as a long (~60 km) streak extending to the east (Figures 1 and 2).

This eruption produced 753 strokes recorded by Vaisala's GLD360 network. Of these, 85 % were in-cloud (IC). The remaining 15 % were cloud-to-ground (CG), with the positive CGs showing higher peak currents than the negative ones. The positive CG lightning dispersed in the same direction as the main eruption cloud (Figure 2B). Figure 2 shows all lightning strokes recorded for the eruption sequence. Most lightning types (positive, negative, IC, CG) were more abundant and generally higher-current close to the volcano, with

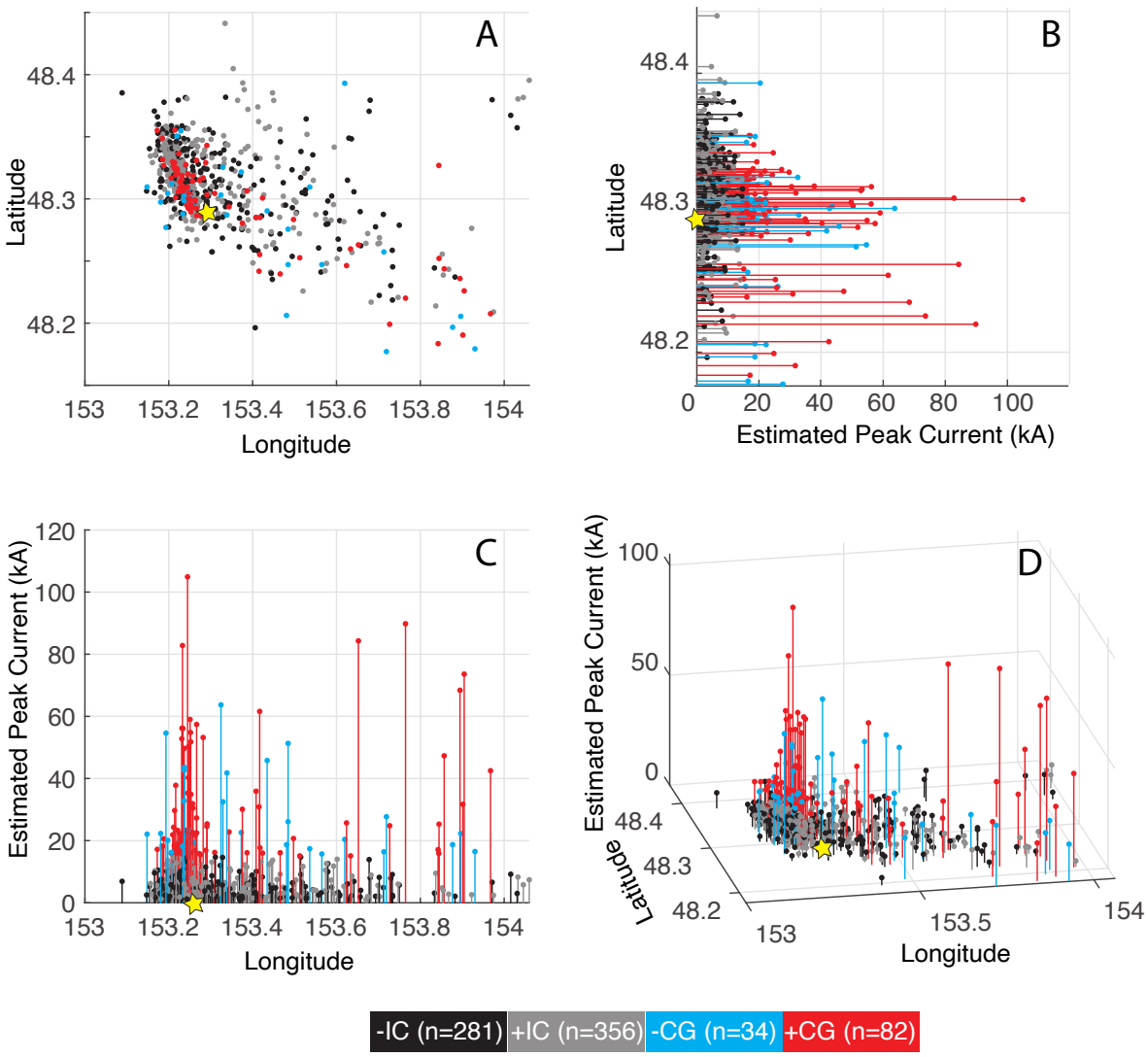

Figure 2: Lightning stroke locations and characteristics detected by the GLD360 network during the 21–22 June 2019 eruption of Raikoke volcano. [A] Lightning locations in decimal degrees; [B,C] estimated peak currents compared to latitude and longitude; [D] Lightning locations in decimal degrees with estimated peak currents shown. Yellow star represents location of Raikoke volcano; colors delineate lightning type (IC = in-cloud, CG = cloud-to-ground) and positive or negative polarity. In legend 'n' refers to the number of detected strokes for the given category.

a rapid decrease with distance. An exception is that positive CG strokes declined more gradually along the main easterly dispersal direction. Stroke counts and percentages for each category are included in Supplementary Material 3.

Figure 3A shows a positive correlation (visually) between the rate of lighting (strokes per 10 min) and plume heights over time. Over the first several hours, each plume rose progressively higher, consistent with increasing mass eruption rates [Sparks et al. 1997; Mastin et al. 2009]. Although the earliest plumes varied in height from about 6–11 km above sea level (Figure 3A), their peak lightning rates stayed relatively constant at ≤10 strokes per 10 minutes. However, the most intense activity during eruptive pulse 7 (plume heights to ~16.5 km) produced a notable increase in the lightning rate, up to ~40 strokes per 10 minutes. The lightning rate then decreased for the smaller, subsequent eruptive pulses. Figure 3B shows that low-current IC strokes dominated the lightning activity overall, with positive ICs occurring most often and following the changes in plume height. CG strokes occurred less often than either positive or negative IC strokes, and negative CG strokes least of all, with some spans of time not having any recorded negative CGs.

Figure 3D shows a positive linear correlation between the radius of the umbrella clouds and spatial footprint of the lightning locations. This correlation has an R^2 of 0.40 and is represented by the equation:

$$E = 4.864(L) + 0.4275 \quad (1)$$

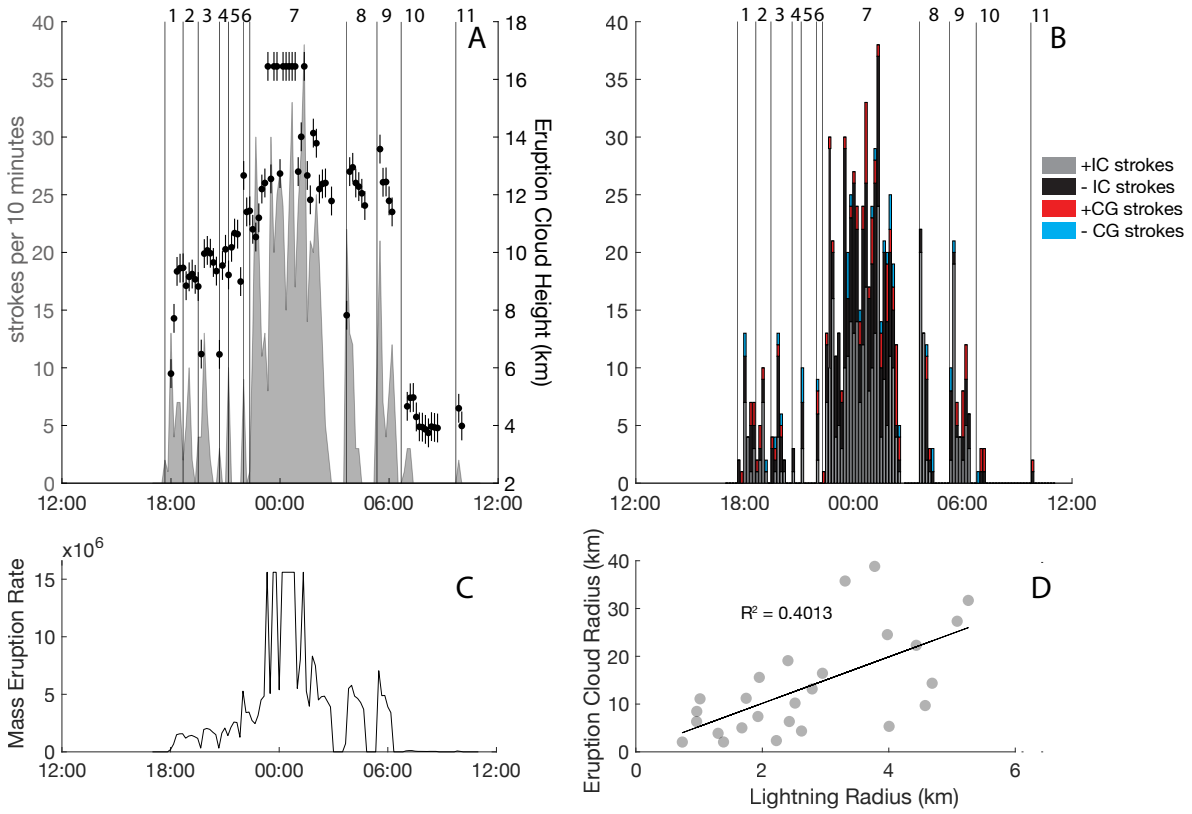

Figure 3: Timeline of Raikoke's volcanic lightning and plume activity from 21–22 June 2019. [A] Lightning stroke rates per 10 minutes (gray, left axis) and maximum plume heights (black dots, right axis); vertical lines delineate the individual eruptive pulses examined in this analysis; [B] lightning stroke rates detailing proportions of positive, negative, in-cloud (IC) and cloud-to-ground (CG) strokes; [C] mass eruption rates (in kg s^{-1}) as calculated from plume heights using an empirical plume height scaling equation; [D] relationship between the size of the lightning footprint ('lightning radius' derived from the area where lightning occurred) and the size of the eruption cloud, shown as area-equivalent circular radius. Note: the x-axes of [A–C] give time (hh:mm) in UTC beginning on 21 June 2019.

where E is the eruption cloud area-equivalent circular radius and L is the area-equivalent circular radius of the convex hull polygon encompassing the lightning locations.

Figure 4 shows rose diagrams for the lightning locations in each eruptive pulse as a histogram binned by the eight main compass directions. This analysis demonstrates that a significant fraction of the lightning occurred northwest of the vent. Only eruptive pulses 4 and 7 created a dominant (or equal) proportion of lightning east of the vent (noting that pulse 4 only had three recorded lightning strokes). Eruptive pulse 7 (the largest) shows lightning concentrated both to the northwest and to the east, following the main easterly dispersal direction of the eruption cloud visible in satellite and photographs (Figure 1B–D).

Previous research on large explosive eruptions that generated globally detected lightning has shown the importance of ice generation for lightning development in the upper regions of the plume [Arason et al. 2011; Van Eaton et al. 2022, and references therein]. To examine if ice development may have influenced charge development in Raikoke volcano's eruptive plumes, we used the 1-D volcanic plume modeling code `Plumeria` [Mastin 2014], exploring the plume heights at which ice formation may have occurred. In Figure 5, panels 5 and 6, we can see that the plumes from the first nine eruptive pulses would have cooled below heterogeneous freezing temperatures (approximately −20 °C) and created ice by the time they reached their maximum height. The height of ice initiation increases for the larger plumes because they are driven by stronger mass eruption rates, which allow them to transport their thermal energy to higher altitudes (i.e. they do not cool as quickly). For example, our model results suggest that the plume from eruptive pulse 7 may not have cooled to freezing temperatures until it reached ~11 km above sea level (Figure 5, panels 5–6, dark green line).

We also examined the start time of each eruptive pulse based on lightning onset and infrasound origin times using the McKee et al. [2021] data recorded by remote infrasound stations ~620 km away (Supplementary Material 1; Table S1). The infrasound-derived estimates of the origin times are picks of the first arrival of a coherent waveform sequence [see Ma-

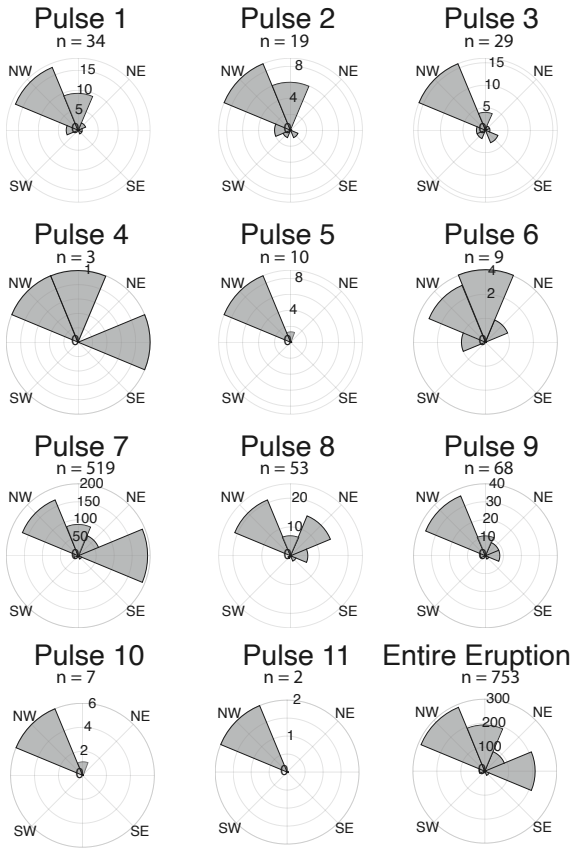

Figure 4: Rose diagrams showing the spatial location of lightning from each of the eruptive pulses examined, binned into eight compass directions (N, NE, E, SE, S, SW, W, NW) with the location of the vent as the center; *n* = number of lightning strokes detected by the GLD360 network.

toza et al. 2011; 2018, for discussion], corrected back to the source using a propagation celerity (source-receiver distance along Earth's surface divided by travel-time) of 0.33 km s^{-1}, which is appropriate for tropospheric propagation, and the range of 620 km [McKee et al. 2021]. This represents one approach to determine eruption onset by the timing of the earliest reliable signal [Coombs et al. 2018]. For five of the eruptive pulses (1, 2, 3, 7, and 9) volcanic lightning gives an earlier onset than (assumed tropospheric) infrasound (by up to ~5 minutes, Supplementary Material 1; Table S1). For the range of 620 km, celerities ranging between 0.33 km s^{-1} (tropospheric), 0.3 km s^{-1} (stratospheric), and 0.28 km s^{-1} (thermospheric) [Brown et al. 2002], result in travel-time differences (uncertainty) on the order of ~5–6 minutes (Supplementary Material 1). Thus, differences in atmospheric path as well as infrasound signal-to-noise effects for emergent signals could potentially account for these timing discrepancies. However, for the other four eruptive pulses (4, 5, 6, and 8), lightning onset occurred after a (fastest possible tropospheric-assumed) infrasound signal origin, within ~3–12 minutes, indicating that volcanic jetting (infrasound signal production) occurred before the onset of the first electrical activity at the source.

4 Discussion

The spatiotemporal development of globally detected volcanic lightning locations during the eruption of Raikoke volcano may help distinguish charging mechanisms and understand how lightning data may be used for monitoring remote eruptions. The lightning stroke rate and plume height timelines in Figure 3 demonstrate that the first six eruptive pulses were short-lived with brief time breaks in between. As shown in Supplementary Material 2, when ash emissions temporarily stopped, the lightning also stopped, even as the ash-rich cloud drifted away. This observation suggests there was insufficient charging in the distal clouds to continue producing lightning, and that the majority of the charging originated close to the volcanic source during these eruptive pulses. In contrast, the longer duration (and more intense) eruptive pulse 7 continued to emit ash for several hours, sustaining a vertical flux into the plume as it expanded and advected away from the vent. This higher-intensity activity (mass eruption rate on the order of ~10^7 kg s^{-1}, Figure 3C) sustained charging processes farther from the vent and expanded the spatial area covered by lightning. The new relationship between umbrella cloud expansion and the growing aerial footprint of lightning activity (Figure 3D and Equation 1) suggests a novel way to estimate the minimum size of an ash cloud in near real-time. This type of simple relationship may also be used to characterize ongoing eruptive activity, which may be particularly useful if other monitoring data are compromised, such as during periods of obscured satellite views.

4.1 Downwind lightning

Satellite images show that the main cloud dispersed east during eruptive pulse 7 (Figure 1B–D). The majority of the lightning also moved eastward (Figure 4). This trend has been observed during previous eruptions like Bogoslof volcano in Alaska [Smith et al. 2018; Van Eaton et al. 2020] and Calbuco volcano in Chile [Van Eaton et al. 2016], suggesting that lightning may commonly follow the main direction of cloud dispersal along with charged particles (i.e. ash, ice, and other hydrometeors). The distribution of high-current CG strokes during this eruption (Figure 2) matches the pattern observed during the 2014 eruption of Kelud volcano in Indonesia [Hargie et al. 2019], wherein the highest-energy lightning was located directly above the vent and dissipated with distance along the main dispersal direction. The population of in-cloud (IC) lightning appears to follow the ash dispersal over short distances to the northwest and over an extended distance to the east-southeast (Figure 2). However, the highest peak current positive CG strokes are located over an extended distance downwind to the east-southeast where the plume reached freezing temperatures. This distribution implies that positive CG strokes may be correlated with long-duration ice development and plume stratification during downwind dispersal of high-altitude plumes. The polarity of CG lightning has been related to storm development and intensification with MacGorman and Burgess [1994] showing that more mesocyclonic winds

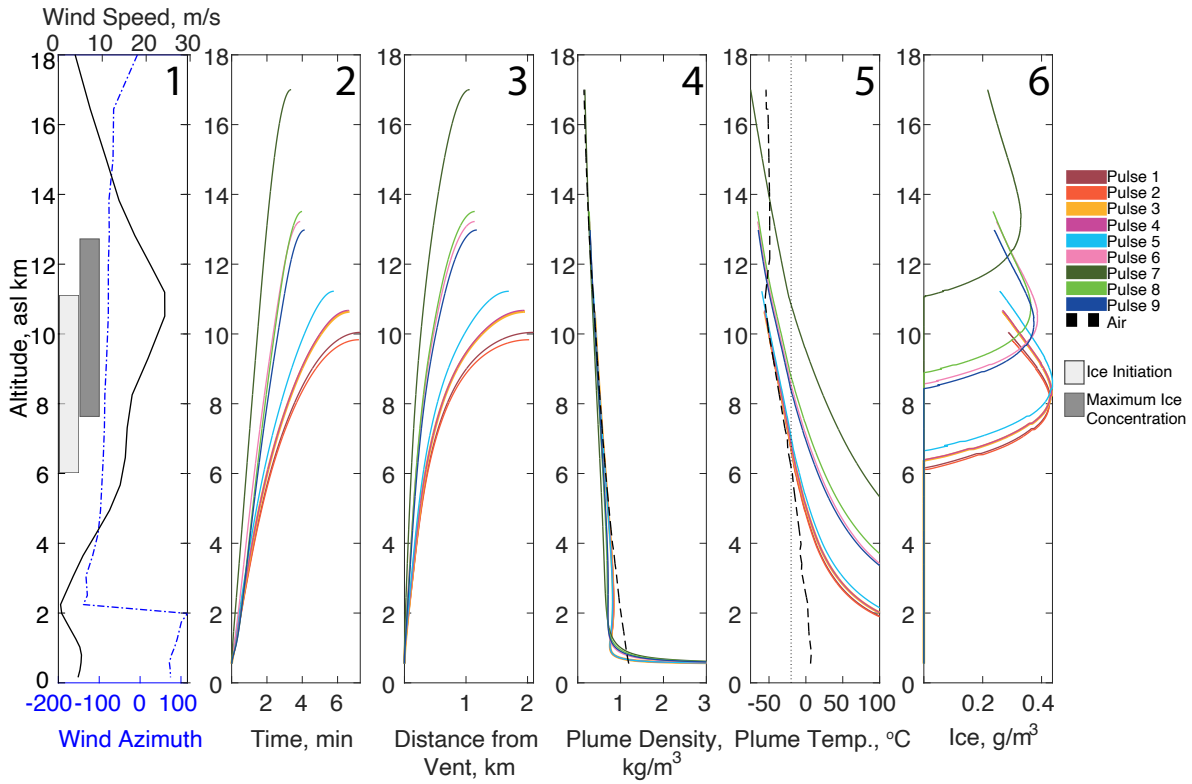

Figure 5: Atmospheric profile and results of one-dimensional volcanic plume modeling using `Plumeria` for the first nine of Raikoke volcano's eruptive pulses (color indicates the eruptive pulse). [1] Atmospheric sounding measurements from Severo-Kurilsk give wind speed in m s^{-1} (black line) and wind azimuth (blue dashed line) showing the direction the wind is coming from in degrees (north is zero). `Plumeria` model results show [2] the time required for each plume to rise to a given height; [3] the horizontal displacement of the plume centerline from the vent due to wind advection; [4] bulk plume density; [5] bulk plume temperature (grey dotted line shows −20 °C); and [6] concentration of ice in the plume. The grey boxes in [1] indicate the full range of modeled ice initiation (6–11 km, light grey) and maximum ice concentrations (8–13 km, dark grey) within the volcanic plumes. Black dashed line in panels [4] and [5] represent the background atmosphere. Eruptive pulses 10 and 11 were not modeled as they had much lower plume heights and the eruption clouds did not reach a temperature of −20 °C and are thus not intercomparable with the larger events.

and high hail concentrations corresponded with more +CG being recorded in severe meteorological storms and that a shift from −CG to +CG can indicate storm intensification. Negative CGs are the dominant polarity for CG in meteorological storms [Dwyer and Uman 2014]. In this eruption, positive polarities dominated the volcanic lightning population (Figure 2). This finding suggests that tracking the evolution of lightning polarity may help distinguish volcanic events from meteorological storms or identify changing processes in the eruption cloud.

4.2 Lightning northwest of Raikoke volcano

The images in Figure 1 also provide insight into the origin of lightning located northwest of the volcano. We infer that the whitish clouds ringing the island during eruptive pulse 7 (Figure 1B) originated from ground-hugging pyroclastic density currents [Smirnov et al. 2021]. These currents lofted ash to altitudes lower than the main plumes where it drifted to the northwest. It stands to reason that the charge generation for this northwest-trending lightning originated from the ground-hugging pyroclastic density currents and associated plumes. Were these lower-altitude charging processes dominated by silicate particle collisions (tribocharging) or ice charging? In this case, we can use wind shear to address the question. Figure 5, panel 1, shows that modeled ice initiated in the Raikoke plumes at ~6–11 km, with the maximum ice concentrations occurring between 8–13 km. These altitudes correspond to winds blowing to the east, whereas lower altitude winds (<2 km) were blowing to the northwest. The observations suggest (ice-free) elutriated ash from ground-hugging pyroclastic density currents made up these northwest clouds and they may have produced lightning mainly by fracto- and tribocharging of the ash particles rather than ice formation. However, one caveat is that the 1-D plume modeling in Figure 5 used source parameters appropriate for hot, vent-derived plumes (initial temperature 1000 °C and plume diameters of

50–150 m). Using inputs better suited to cooler, lofted ash rising from pyroclastic density currents over a wider area may have resulted in models showing ice nucleating lower in the plume.

Our modeling results in Figure 5 suggest that all nine of the eruptive pulses modeled were capable of forming ice in the upper troposphere; collisional, non-inductive ice charging (similar to that seen in thunderstorms) requires liquid water as well as ice. A 'mixed-phase region' within the eruption cloud is the ideal scenario for non-inductive charging leading to lightning production, as shown during the eruptions of Bogoslof volcano, Alaska, in 2016–2017 [Van Eaton et al. 2020], Anak Krakatau, Indonesia, in 2018 [Prata et al. 2020], and Taal, Philippines, in 2020 [Van Eaton et al. 2022]. However, those eruptions involved the addition of external water from crater lakes or seawater. Our `Plumeria` model runs for Raikoke volcano did not include external water and, as a result, show no mixed-phase (liquid water-rich) regions developing within the plumes (Figure 5, panel 6). Our initial analysis suggested that the Raikoke eruption was comparatively 'dry' (lacking external water involvement) due to the subaerial vent and dominance of brownish, ash-rich clouds in satellite (e.g. Figure 1C). Yet, the work of Smirnov et al. [2021] has suggested otherwise. Their study infers that the fine grain size of the ash deposits and uniformly crystal-rich, bubble-poor pyroclasts required magma-water interaction to trigger such explosive activity. Based on our observations from visible satellite images and photographs (e.g. Figure 1), we cannot rule out magma-water interaction during the Raikoke eruption. We suggest that, if present, the water proportions were modest compared to some of the more extreme recent examples. For example, the shallow submarine eruption of Anak Krakatau [Cutler et al. 2022], which reached similar maximum plume heights as Raikoke, produced much lighter-colored, water-rich clouds overall [Prata et al. 2020]. A detailed examination of the relative roles of external water during these eruptions, and the effects on lightning production, would be a rich area for future investigation.

5 Conclusions

We examined the eruption cloud characteristics, volcanic lightning (as detected by the GLD360 lightning network), and source parameters of the eruption of Raikoke volcano in the Kuril Islands from 21–22 June 2019. Our overall goal was to determine how volcanic lightning may provide insights into the dynamics of a developing eruption cloud. Using spatial and temporal characteristics along with weather data and volcanic plume modeling, we explored electrical charging mechanisms (silicate vs. ice charging) in different regions of the eruption clouds. In this case, it was plausible that ice formation played an important role in lightning generation for each of the nine main eruptive pulses. However, we speculate that the lower-altitude cloud rising from pyroclastic density currents (and dispersing northwest) may have charged primarily by silicate particle interactions because it may not have risen high enough to have any water in it freeze. We found that lightning locations tracked dispersal patterns of this ash cloud lofted from ground-hugging pyroclastic density currents, in addition to the larger, vent-derived eruption plumes. We also demonstrated a positive relationship between the expanding umbrella clouds and the growing spatial footprint of lightning.

We suggest that future work addressing the distribution of lightning peak currents may be valuable for developing monitoring alarms that aim to distinguish volcanic from non-volcanic clouds, as it stands to reason that a meteorological storm would not show the same spatial distribution (with the highest peak currents centered on the volcano, Figure 2). Further analysis of volcanic lightning polarity and type (in-cloud or cloud-to-ground) may also be beneficial for assessing lightning hazards in highly populated regions, as a recent eruption of Taal volcano, Philippines, suggested that volcanoes may dramatically increase the local lightning exposure risk [Van Eaton et al. 2022]. It has been previously established that globally detected volcanic lightning can help identify the onset of ash-rich explosive eruptions, but this work now demonstrates that spatial patterns in two-dimensional lightning locations may also be used to track the location and growth of eruption clouds and perhaps distinguish lower-level ash clouds, which pose distinct hazards.

Author Contributions

CMS conceived of the project, analyzed the data, and wrote the manuscript. AVE contributed to discussion and draft writing and reviewing. LM provided technical guidance on Plumeria and reviewed drafts. DS provided discussion and reviewed drafts. RSM, KM, and SM provided infrasound data, discussion, wrote the infrasound analysis section, and reviewed drafts.

Acknowledgements

CMS acknowledges NSF grant EAR-PF-1855153. RSM acknowledges NSF grant EAR-1847736. Any use of trade, firm, or product names is for descriptive purposes only and does not imply endorsement by the U.S. Government. We thank Thomas Farges, Caron Vossen, and Lis Gallant for their reviews that greatly improved the clarity of the manuscript. We would like to thank Rodrigo de Negri Leiva, Jelle Assink, and Anna Perttu for infrasound data access, and Hans Schwaiger for assistance with ERA-interim data. We thank Ryan Said for providing information on uncertainties in the lightning locations. CMS would also like to acknowledge the CIDER program and all members of the USGS virtual writing group for the motivation to complete this project during the covid-19 pandemic.

Data Availability

Lightning strokes, flashes, plume heights, and model inputs and output are included in Supplementary Material 1, Supplementary Material 2, and Supplementary Material 3. Raw lightning data from GLD360 are available upon request from Vaisala, Inc. Himawari-8 satellite images are freely available from the Satellite Data Services group at the University of Wisconsin-Madison Space Science and Engineering Center.

References

Arason, P., A. J. Bennett, and L. E. Burgin (2011). "Charge mechanism of volcanic lightning revealed during the 2010 eruption of Eyjafjallajökull". *Journal of Geophysical Research* 116. DOI: 10.1029/2011jb008651.

Behnke, S. A. and S. R. McNutt (2014). "Using lightning observations as a volcanic eruption monitoring tool". *Bulletin of Volcanology* 76(8). DOI: 10.1007/s00445-014-0847-1.

Behnke, S. A., R. J. Thomas, S. R. McNutt, D. J. Schneider, P. R. Krehbiel, W. Rison, and H. E. Edens (2013). "Observations of volcanic lightning during the 2009 eruption of Redoubt Volcano". *Journal of Volcanology and Geothermal Research* 259, pages 214–234. DOI: 10.1016/j.jvolgeores.2011.12.010.

Biagi, C. J., K. L. Cummins, K. E. Kehoe, and E. P. Krider (2007). "National Lightning Detection Network (NLDN) performance in southern Arizona, Texas, and Oklahoma in 2003–2004". *Journal of Geophysical Research* 112(D5). DOI: 10.1029/2006jd007341.

Brown, D. J., C. N. Katz, R. L. Bras, M. P. Flanagan, J. Wang, and A. K. Gault (2002). "Infrasonic Signal Detection and Source Location at the Prototype International Data Centre". *Pure and Applied Geophysics* 159(5), pages 1081–1125. DOI: 10.1007/s00024-002-8674-2.

Buiat, M., F. Porcù, and S. Dietrich (2017). "Observing relationships between lightning and cloud profiles by means of a satellite-borne cloud radar". *Atmospheric Measurement Techniques* 10(1), pages 221–230. DOI: 10.5194/amt-10-221-2017.

Carey, L. D., E. V. Schultz, C. J. Schultz, W. Deierling, W. A. Petersen, A. L. Bain, and K. E. Pickering (2019). "An Evaluation of Relationships between Radar-Inferred Kinematic and Microphysical Parameters and Lightning Flash Rates in Alabama Storms". *Atmosphere* 10(12), page 796. DOI: 10.3390/atmos10120796.

Coombs, M. L., A. G. Wech, M. M. Haney, J. J. Lyons, D. J. Schneider, H. F. Schwaiger, K. L. Wallace, D. Fee, J. T. Freymueller, J. R. Schaefer, and G. Tepp (2018). "Short-Term Forecasting and Detection of Explosions During the 2016–2017 Eruption of Bogoslof Volcano, Alaska". *Frontiers in Earth Science* 6. DOI: 10.3389/feart.2018.00122.

Cummins, K. L. and M. J. Murphy (2009). "An Overview of Lightning Locating Systems: History, Techniques, and Data Uses, With an In-Depth Look at the U.S. NLDN". *IEEE Transactions on Electromagnetic Compatibility* 51(3), pages 499–518. DOI: 10.1109/temc.2009.2023450.

Cutler, K. S., S. F. Watt, M. Cassidy, A. L. Madden-Nadeau, S. L. Engwell, M. Abdurrachman, M. E. Nurshal, D. R. Tappin, S. N. Carey, A. Novellino, C. Hayer, J. E. Hunt, S. J. Day, S. T. Grilli, I. A. Kurniawan, and N. Kartadinata (2022). "Downward-propagating eruption following vent unloading implies no direct magmatic trigger for the 2018 lateral collapse of Anak Krakatau". *Earth and Planetary Science Letters* 578, page 117332. DOI: 10.1016/j.epsl.2021.117332.

Dee, D. P., S. M. Uppala, A. J. Simmons, P. Berrisford, P. Poli, S. Kobayashi, U. Andrae, M. A. Balmaseda, G. Balsamo, P. Bauer, P. Bechtold, A. C. M. Beljaars, L. van de Berg, J. Bidlot, N. Bormann, C. Delsol, R. Dragani, M. Fuentes, A. J. Geer, L. Haimberger, S. B. Healy, H. Hersbach, E. V. Hólm, L. Isaksen, P. Kållberg, M. Köhler, M. Matricardi, A. P. McNally, B. M. Monge-Sanz, J.-J. Morcrette, B.-K. Park, C. Peubey, P. de Rosnay, C. Tavolato, J.-N. Thépaut, and F. Vitart (2011). "The ERA-Interim reanalysis: configuration and performance of the data assimilation system". *Quarterly Journal of the Royal Meteorological Society* 137(656), pages 553–597. DOI: 10.1002/qj.828.

Degterev, A. and M. Chibisova (2020). "The volcanic activity at the Kuril Islands in 2019". *Geosystems of Transition Zones* 4(1), pages 93–102. DOI: 10.30730/2541-8912.2020.4.1.093-102.

Deierling, W., W. A. Petersen, J. Latham, S. Ellis, and H. J. Christian (2008). "The relationship between lightning activity and ice fluxes in thunderstorms". *Journal of Geophysical Research* 113(D15). DOI: 10.1029/2007jd009700.

Dwyer, J. R. and M. A. Uman (2014). "The physics of lightning". *Physics Reports* 534(4), pages 147–241. DOI: 10.1016/j.physrep.2013.09.004.

Firstov, P., O. Popov, M. Lobacheva, D. Budilov, and R. Akbashev (2020). "Wave perturbations in the atmosphere accompanying the eruption of the Raykoke volcano (Kuril Islands) June 21–22, 2019". *Geosystems of Transition Zones* 4(1), pages 71–92. DOI: 10.30730/2541-8912.2020.4.1.071-081.082-092.

Girina, O., E. Loupian, I. Uvarov, and L. Kramareva (2019). "Raikoke volcano eruption on 21 June 2019". *Sovremennye problemy distantsionnogo zondirovaniya Zemli iz kosmosa* 16(3), pages 303–307. DOI: 10.21046/2070-7401-2019-16-3-303-307.

Hargie, K. A., A. R. Van Eaton, L. G. Mastin, R. H. Holzworth, J. W. Ewert, and M. Pavolonis (2019). "Globally detected volcanic lightning and umbrella dynamics during the 2014 eruption of Kelud, Indonesia". *Journal of Volcanology and Geothermal Research* 382, pages 81–91. DOI: 10.1016/j.jvolgeores.2018.10.016.

Hoblitt, R. P. (1994). "An experiment to detect and locate lightning associated with eruptions of Redoubt Volcano". *Journal of Volcanology and Geothermal Research* 62(1-4), pages 499–517. DOI: 10.1016/0377-0273(94)90049-3.

Horváth, Á., O. A. Girina, J. L. Carr, D. L. Wu, A. A. Bril, A. A. Mazurov, D. V. Melnikov, G. A. Hoshyaripour, and S. A. Buehler (2021). "Geometric estimation of volcanic eruption column height from GOES-R near-limb imagery – Part 2: Case studies". *Atmospheric Chemistry and Physics* 21(16), pages 12207–12226. DOI: 10.5194/acp-21-12207-2021.

James, M. R., L. Wilson, S. J. Lane, J. S. Gilbert, T. A. Mather, R. G. Harrison, and R. S. Martin (2008). "Electrical Charging of Volcanic Plumes". *Space Science Reviews* 137(1-4), pages 399–418. DOI: 10.1007/s11214-008-9362-z.

Kloss, C., G. Berthet, P. Sellitto, F. Ploeger, G. Taha, M. Tidiga, M. Eremenko, A. Bossolasco, F. Jégou, J.-B. Renard, and B. Legras (2021). "Stratospheric aerosol layer perturbation caused by the 2019 Raikoke and Ulawun eruptions and their radiative forcing". *Atmospheric Chemistry and Physics* 21(1), pages 535–560. DOI: 10.5194/acp-21-535-2021.

Levin, B. V., I. V. Melekestsev, A. V. Rybin, N. G. Razzhigaeva, E. A. Kravchunovskaya, P. E. Izbekov, A. V. Degtyarev, R. V. Zharkov, D. N. Kozlov, M. V. Chibisova, I. I. Vlasov, V. B. Guryanov, I. G. Koroteev, A. A. Kharlamov, and B. McInnes (2010). "Expedition "Sarychev Peak Volcano-2010" (Kuril Islands)". *Far Eastern Branch of the Russian Academy of Sciences* 6, pages 151–158. [in Russian with English abstract].

MacGorman, D. R. and D. W. Burgess (1994). "Positive Cloud-to-Ground Lightning in Tornadic Storms and Hailstorms". *Monthly Weather Review* 122(8), pages 1671–1697. DOI: 10.1175/1520-0493(1994)122<1671:pctgli>2.0.co;2.

Mastin, L. G. (2007). "A user-friendly one-dimensional model for wet volcanic plumes". *Geochemistry, Geophysics, Geosystems* 8(3). DOI: 10.1029/2006gc001455.

– (2014). "Testing the accuracy of a 1-D volcanic plume model in estimating mass eruption rate". *Journal of Geophysical Research: Atmospheres* 119(5), pages 2474–2495. DOI: 10.1002/2013jd020604.

Mastin, L. G., M. Guffanti, R. Servranckx, P. Webley, S. Barsotti, K. Dean, A. Durant, J. Ewert, A. Neri, W. Rose, D. Schneider, L. Siebert, B. Stunder, G. Swanson, A. Tupper, A. Volentik, and C. Waythomas (2009). "A multidisciplinary effort to assign realistic source parameters to models of volcanic ash-cloud transport and dispersion during eruptions". *Journal of Volcanology and Geothermal Research* 186(1–2), pages 10–21. DOI: 10.1016/j.jvolgeores.2009.01.008.

Mather, T. A. and R. G. Harrison (2006). "Electrification of volcanic plumes". *Surveys in Geophysics* 27(4), pages 387–432. DOI: 10.1007/s10712-006-9007-2.

Matoza, R. S., D. Fee, D. N. Green, A. Le Pichon, J. Vergoz, M. M. Haney, T. D. Mikesell, L. Franco, O. A. Valderrama, M. R. Kelley, K. McKee, and L. Ceranna (2018). "Local, Regional, and Remote Seismo-acoustic Observations of the April 2015 VEI 4 Eruption of Calbuco Volcano, Chile". *Journal of Geophysical Research: Solid Earth* 123(5), pages 3814–3827. DOI: 10.1002/2017jb015182.

Matoza, R. S., A. Le Pichon, J. Vergoz, P. Herry, J.-M. Lalande, H.-i. Lee, I.-Y. Che, and A. Rybin (2011). "Infrasonic observations of the June 2009 Sarychev Peak eruption, Kuril Islands: Implications for infrasonic monitoring of remote explosive volcanism". *Journal of Volcanology and Geothermal Research* 200(1–2), pages 35–48. DOI: 10.1016/j.jvolgeores.2010.11.022.

McKee, K., C. M. Smith, K. Reath, E. Snee, S. Maher, R. S. Matoza, S. Carn, L. Mastin, K. Anderson, D. Damby, D. C. Roman, A. Degterev, A. Rybin, M. Chibisova, J. D. Assink, R. de Negri Leiva, and A. Perttu (2021). "Evaluating the state-of-the-art in remote volcanic eruption characterization Part I: Raikoke volcano, Kuril Islands". *Journal of Volcanology and Geothermal Research* 419, page 107354. DOI: 10.1016/j.jvolgeores.2021.107354.

McNutt, S. R. and E. R. Williams (2010). "Volcanic lightning: global observations and constraints on source mechanisms". *Bulletin of Volcanology* 72(10), pages 1153–1167. DOI: 10.1007/s00445-010-0393-4.

Méndez Harper, J., L. Courtland, J. Dufek, and J. McAdams (2020). "Microphysical Effects of Water Content and Temperature on the Triboelectrification of Volcanic Ash on Long Time Scales". *Journal of Geophysical Research: Atmospheres* 125(14). DOI: 10.1029/2019jd031498.

Nicoll, K., M. Airey, C. Cimarelli, A. Bennett, G. Harrison, D. Gaudin, K. Aplin, K. L. Koh, M. Knuever, and G. Marlton (2019). "First In Situ Observations of Gaseous Volcanic Plume Electrification". *Geophysical Research Letters* 46(6), pages 3532–3539. DOI: 10.1029/2019gl082211.

Prata, A. T., A. Folch, A. J. Prata, R. Biondi, H. Brenot, C. Cimarelli, S. Corradini, J. Lapierre, and A. Costa (2020). "Anak Krakatau triggers volcanic freezer in the upper troposphere". *Scientific Reports* 10(1). DOI: 10.1038/s41598-020-60465-w.

Rudlosky, S. D. and H. E. Fuelberg (2010). "Pre- and Postupgrade Distributions of NLDN Reported Cloud-to-Ground Lightning Characteristics in the Contiguous United States". *Monthly Weather Review* 138(9), pages 3623–3633. DOI: 10.1175/2010mwr3283.1.

Rueden, C. T., J. Schindelin, M. C. Hiner, B. E. DeZonia, A. E. Walter, E. T. Arena, and K. W. Eliceiri (2017). "ImageJ2: ImageJ for the next generation of scientific image data". *BMC Bioinformatics* 18(1). DOI: 10.1186/s12859-017-1934-z.

Said, R. K., U. S. Inan, and K. L. Cummins (2010). "Long-range lightning geolocation using a VLF radio atmospheric waveform bank". *Journal of Geophysical Research* 115(D23). DOI: 10.1029/2010jd013863.

Said, R. K. and M. J. Murphy (2016). "GLD360 upgrade: Performance analysis and applications." In: *Proceedings of the 24th International Lightning Detection Conference & 6th International Lightning Meteorology Conference , San Diego, California, April 2016*. https://www.vaisala.com/sites/default/files/documents/Ryan%20Said%20and%20Martin%20Murphy.%20GLD360%20Upgrade%20Performance%20Analysis%20and%20Applications.pdf.

Saunders, C. P. R., H. Bax-norman, C. Emersic, E. E. Avila, and N. E. Castellano (2006). "Laboratory studies of the effect of cloud conditions on graupel/crystal charge transfer in thunderstorm electrification". *Quarterly Journal of the Royal Meteorological Society* 132(621), pages 2653–2673. DOI: 10.1256/qj.05.218.

Schultz, C. J., L. D. Carey, E. V. Schultz, and R. J. Blakeslee (2017). "Kinematic and Microphysical Significance of Lightning Jumps versus Nonjump Increases in Total Flash Rate". *Weather and Forecasting* 32(1), pages 275–288. DOI: 10.1175/waf-d-15-0175.1.

Schultz, C. J., W. A. Petersen, and L. D. Carey (2011). "Lightning and Severe Weather: A Comparison between Total and Cloud-to-Ground Lightning Trends". *Weather and Forecasting* 26(5), pages 744–755. DOI: 10.1175/waf-d-10-05026.1.

Smirnov, S., I. Nizametdinov, T. Timina, A. Kotov, V. Sekisova, D. Kuzmin, E. Kalacheva, V. Rashidov, A. Rybin, A. Lavrenchuk, A. Degterev, I. Maksimovich, and A. Abersteiner (2021). "High explosivity of the June 21, 2019 eruption of Raikoke volcano (Central Kuril Islands); mineralogical and petrological constraints on the pyroclastic materials". *Journal of Volcanology and Geothermal Research* 418, page 107346. DOI: 10.1016/j.jvolgeores.2021.107346.

Smith, C. M., A. R. Van Eaton, R. Said, and R. H. Holzworth (2018). "Volcanic lightning as a monitoring tool during the 2016-2017 eruption of Bogoslof Volcano, AK." In: *Proceedings of the International Lightning Detection Conference/ International Lightning Meteorology Conference, 12–15 March, Fort Lauderdale, Florida, USA, 1–5.* https://www.vaisala.com/sites/default/files/documents/Volcanic%20lightning%20as%20monitoring%20tool%20during%202016-2017%20eruption%20of%20Bogoslof%20Volcano%20AK_C.M.%20Smith%20et%20al.pdf.

Smith, C. M., D. Gaudin, A. R. Van Eaton, S. A. Behnke, S. Reader, R. J. Thomas, H. Edens, S. R. McNutt, and C. Cimarelli (2021). "Impulsive Volcanic Plumes Generate Volcanic Lightning and Vent Discharges: A Statistical Analysis of Sakurajima Volcano in 2015". *Geophysical Research Letters* 48(11). DOI: 10.1029/2020gl092323.

Sparks, R. S. J., M. I. Bursik, S. N. Carey, J. Gilbert, L. S. Glaze, H. Sigurdsson, and A. W. Woods (1997). *Volcanic plumes*. Wiley. ISBN: 0471939013.

Van Eaton, A. R., Á. Amigo, D. Bertin, L. G. Mastin, R. E. Giacosa, J. González, O. Valderrama, K. Fontijn, and S. A. Behnke (2016). "Volcanic lightning and plume behavior reveal evolving hazards during the April 2015 eruption of Calbuco volcano, Chile". *Geophysical Research Letters* 43(7), pages 3563–3571. DOI: 10.1002/2016gl068076.

Van Eaton, A. R., D. J. Schneider, C. M. Smith, M. M. Haney, J. J. Lyons, R. Said, D. Fee, R. H. Holzworth, and L. G. Mastin (2020). "Did ice-charging generate volcanic lightning during the 2016–2017 eruption of Bogoslof volcano, Alaska?" *Bulletin of Volcanology* 82(3). DOI: 10.1007/s00445-019-1350-5.

Van Eaton, A. R., C. M. Smith, M. Pavolonis, and R. Said (2022). "Eruption dynamics leading to a volcanic thunderstorm—The January 2020 eruption of Taal volcano, Philippines". *Geology* 50(4), pages 491–495. DOI: 10.1130/g49490.1.

Williams, E. R., M. E. Weber, and R. E. Orville (1989). "The relationship between lightning type and convective state of thunderclouds". *Journal of Geophysical Research* 94(D11), page 13213. DOI: 10.1029/jd094id11p13213.

Woodhouse, M. J. and S. A. Behnke (2014). "Charge structure in volcanic plumes: a comparison of plume properties predicted by an integral plume model to observations of volcanic lightning during the 2010 eruption of Eyjafjallajökull, Iceland". *Bulletin of Volcanology* 76(8). DOI: 10.1007/s00445-014-0828-4.